Sensors and Actuators B 155 (2011) 232–238

Contents lists available at ScienceDirect

Sensors and Actuators B: Chemical

journal homepage: www.elsevier.com/locate/snb

Ethanol sensing properties of $LaCo_xFe_{1-x}O_3$ nanoparticles: Effects of calcination temperature, Co-doping, and carbon nanotube-treatment

Caihui Feng[a], Shengping Ruan[a], Jiajing Li[b], Bo Zou[b], Junyu Luo[a], Weiyou Chen[a], Wei Dong[a,*], Fengqing Wu[b,*]

[a] State Key Laboratory on Integrated Optoelectronics, College of Electronic Science and Engineering, Jilin University, Changchun 130012, PR China
[b] College of Chemistry, Jilin University, Changchun 130012, PR China

ARTICLE INFO

Article history:
Received 27 July 2010
Received in revised form
24 November 2010
Accepted 25 November 2010
Available online 3 December 2010

Keywords:
Gas sensors
Nanomaterials
Nanostructures
One dimension
Perovskite
Carbon nanotubes

ABSTRACT

$LaCo_xFe_{1-x}O_3$ nanoparticles ($x = 0$, 0.1, 0.2, and 0.3) are prepared by a sol–gel method, and the effects of calcination temperature, Co-doping, and carbon nanotube (CNT)-treatment on their ethanol sensing properties are investigated. The highest response is found based on the $LaCo_{0.1}Fe_{0.9}O_3$ nanoparticles calcined at 600 °C, and the sensing properties of this sample can be further improved by adding CNT in the precursor. The responses of un-treated and CNT-treated $LaCo_{0.1}Fe_{0.9}O_3$ nanoparticles are about 120.1 and 137.3–500 ppm ethanol at 140 °C, respectively. Simultaneously, by CNT -treatment, the response time is decreased from 56 to 10 s, and the recovery time is decreased from 95 to 35 s. The results not only make $LaCo_{0.1}Fe_{0.9}O_3$ nanoparticles good candidates for fabricating practical gas sensors, but also provide a possible route for employing CNTs as a pore-forming agent.

1. Introduction

Due to their variable structure and chemical composition, perovskite type oxides with general formula ABO_3 have so far attracted great interest in many applications such as fuel cells, catalysts, and chemical sensors [1–5]. Sensors based on the ABO_3-type composite oxides have an advantage of high stability, and their response and selectivity can be effectively controlled by selecting suitable A and B atoms or chemical dopant as $A'_xA_{1-x}B'_xB_{1-x}O_3$ materials [6,7]. The perovskite type $LaFeO_3$ is one of the most valuable ABO_3-type functional materials, especially in gas sensor field [8–10]. $LaFeO_3$ is a p-type semiconducting oxide, and its resistance will increase when it is exposed to a reducing gas. Usually, pure $LaFeO_3$ can not be used as the sensing material directly because its resistance is too large to match the amplifying circuits. Thus many metals are chosen and doped in $LaFeO_3$ to decrease its resistance [11,12]. Co has been proved to be an efficient dopant for decreasing the resistance of $LaFeO_3$, and many $LaCo_xFe_{1-x}O_3$ related materials have been proved to own excellent sensing properties, such as high response and good selectivity [13–17]. Hitherto, preparation of $LaCo_xFe_{1-x}O_3$ and related compounds has been achieved by many methods, including sol–gel, combustion synthesis, and hydrothermal synthesis. And the optimal doping rate (x) is found to strongly depend on the synthesis method, sensor structure, micromorphology and crystal structure [13–17].

In recent ten years, inspired by their exceptional sensing properties, many one dimensional (1D) semiconducting oxides have been studied as gas sensing materials [18–21]. 1D nanostructure materials are strong candidates for gas sensing because their large surface-to-volume ratio and the congruence of the carrier screening length with their lateral dimensions will make them highly sensitive and efficient transducers of surface chemical processes into electrical signals [22]. Carbon nanotube (CNT) is one of the most important 1D sensing materials with high yield and low price [23–25]. Since it was discovered in 1991, over 30,000 scientific reports have been published on their gas sensor applications [25]. For majority investigations, CNTs with different morphologies and structures are studied as the sensing materials directly. Some groups also use them to control the resistance or surface area of the sensing materials [26]. However, with an eye to its uniform nanostructure and low oxidation temperature (500–700 °C) [27], CNTs may also be used as an efficient pore-forming agent.

In this paper, we synthesize $LaCo_xFe_{1-x}O_3$ nanocrystalline materials ($x = 0$, 0.1, 0.2, and 0.3) and investigate their ethanol sensing properties. The optimal calcination temperature and doping rate are provided. Most importantly, we believe that our method

* Corresponding authors. Tel.: +86 431 85168242; fax: +86 431 85168242.
E-mail addresses: dongw@jlu.edu.cn (W. Dong), jluhuihui@gmail.com (F. Wu).

0925-4005/$ – see front matter © 2010 Elsevier B.V. All rights reserved.
doi:10.1016/j.snb.2010.11.053

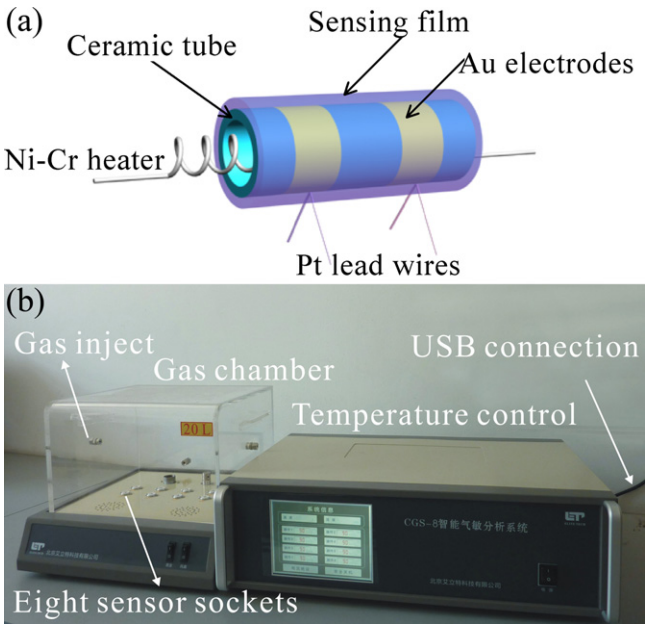

Fig. 1. Schematic image of $LaCo_xFe_{1-x}O_3$ sensor (a) and sensing measuring equipment (b).

can offer a possible platform to understand and employ CNTs as the pore-forming agent in sensing materials.

2. Experimental

2.1. Preparation of materials

$La(NO_3)_3{\cdot}6H_2O$, $Fe(NO_3)_3{\cdot}9H_2O$, $Co(NO_3)_2{\cdot}6H_2O$, and citric acid (analytical grade reagents) were purchased from Beijing Chemicals Co., Ltd. CNTs (LMWNT S-10 d < 10 nm, L = 5–15 um) were purchased from Shenzhen Nanotech Port Co., Ltd. The deionized water with a resistivity of 18.0 MΩ cm^{-1} was used in all experiments.

$LaCo_xFe_{1-x}O_3$ (x = 0, 0.1, 0.2, and 0.3) nanoparticles were prepared by a sol–gel method. Typically, $La(NO_3)_3{\cdot}6H_2O$ (12.99 g), $Fe(NO_3)_3{\cdot}9H_2O$ (12.12, 10.91, 9.7, and 8.48 g), and $Co(NO_3)_2{\cdot}6H_2O$ (0, 0.87, 1.75, and 2.62 g) were weighed and dissolved in deionized water, then the three solutions were mixed together, and citric acid was added into the mixed solution at a ratio of $m(la^{3+} + Fe^{3+} + Co^{2+})$:m(citric) = 1:1.2. The solutions were then heated at 80 °C with constantly stirring to evaporate deionized water until a sol was obtained. The sol was firstly dried into a gel, and then dried into pieces under an infrared lamp. After that, the pieces were ground to form fine powders by a hand-mill. Finally the powders were calcined at 400, 500, 600, 700, and 800 °C for 2 h to obtain perovskite-type nanoparticles. CNT-treated sample was prepared by adding 5 wt.% CNT in the $LaCo_{0.1}Fe_{0.9}O_3$ precursor pieces and then ground and calcined at 600 °C.

2.2. Measurement

The as-synthesized sample was mixed with deionized water in a weight ratio of 100:25 and ground in a mortar for 3 h to form a paste. The paste was then coated on a ceramic tube to form a sensing film (with a thickness of about 300 μm) on which a pair of Au electrodes was previously printed. Pt lead wires attaching to these electrodes were used as electrical contacts. After the ceramic tube was calcined at 300 °C for 2 h, a Ni–Cr heating wire was inserted in the tube as a heater for controlling the operating temperature [28]. The structure of the sensor is shown in Fig. 1(a).

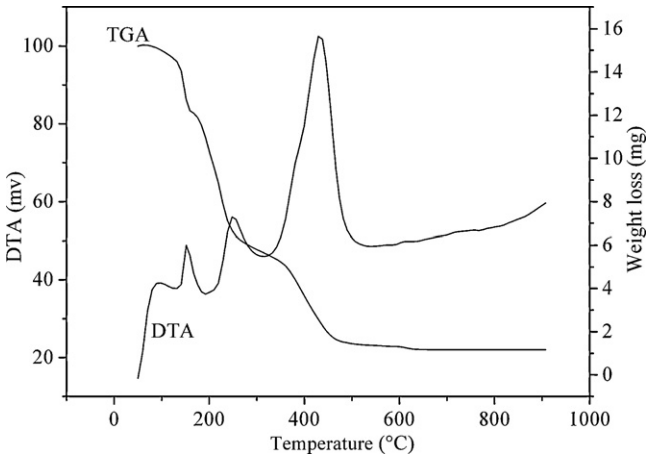

Fig. 2. DTA and TGA curves of $LaCo_{0.1}Fe_{0.9}O_3$ precursor.

Gas sensing properties were measured by a CGS-8 (Chemical gas sensor-8) intelligent gas sensing analysis system (Beijing Elite Tech Co., Ltd., China) (Fig. 1(b)) [29]. The sensors were pre-heated at different operating temperatures for about 30 min. When the resistances of all the sensors were stable, saturated target gas was injected into the test chamber (20 L in volume) by a microinjector through a rubber plug. The saturated target gas was mixed with air (relative humidity was about 25%) by two fans in the analysis system. After the sensor resistances reached a new constant value, the test chamber was opened to recover the sensors in air. All the measurements were performed in a laboratory fume hood. The sensor resistance and response values were acquired by the analysis system automatically. The response value (R) was defined as R = Rg/Ra, where Ra and Rg denoted the sensor's resistance in the absence and in the presence of the target gases. The time taken by the sensor to achieve 90% of the total resistance change was defined as the response time in the case of response (target gas adsorption) or the recovery time in the case of recovery (target gas desorption).

The thermal decomposition behaviors of the $LaCo_xFe_{1-x}O_3$ precursors were examined by means of differential thermal analysis (DTA) and thermal gravimetric analysis (TGA), using a Melttler Toledo 825^e thermal analyzer. The precursors were heated up to 900 °C in air at a scan rate of 10 °C/min. The crystal structure of the samples was examined by X-ray diffraction (XRD) on a Shimadzu XRD-6000 diffractometer with Cu Kα radiation. The current and voltage during the measurements were 30 mA and 40 kV, respectively. The morphology of the samples was observed using a scanning electron microscope (SEM) (XL30 ESEM FEG). Brunauer–Emmett–Teller (BET) surface area and pore size distribution of the samples were measured by a nitrogen adsorption–desorption analyzer (Quantachrome Autosorb-1C). We calculated specific surface area S_{BET} by using the BET method, and determined pore size distribution by applying the Barrett–Joyner–Halenda (BJH) model.

3. Results and discussion

3.1. Effect of calcination temperature

Fig. 2 shows the DTA and TGA curves of $LaCo_{0.1}Fe_{0.9}O_3$ precursor (before calcination). The DTA curve exhibits three exothermic peaks at 150.8, 248.5, 432.7 °C, and a weak exothermic peak at 602 °C, respectively. The first exothermic peak at 150.8 °C is attributed to the decomposition of the dissociative citric acid in the $LaCo_{0.1}Fe_{0.9}O_3$ precursor. The second exothermic peak at 248.5 °C refers to the combustion of the citric acid. The third exother-

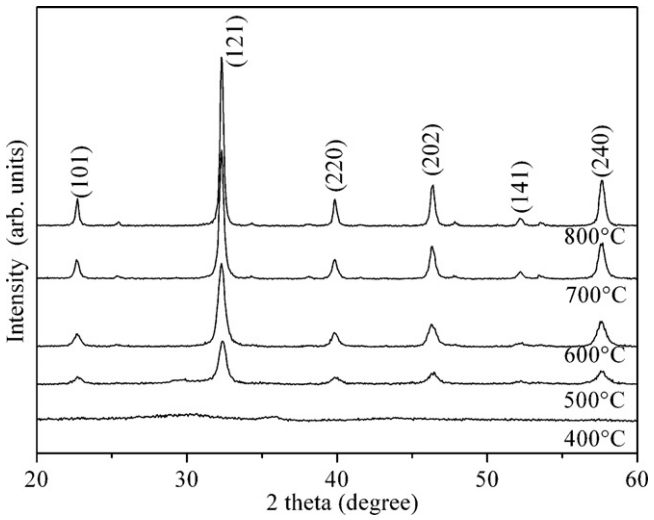

Fig. 3. XRD patterns of $LaCo_{0.1}Fe_{0.9}O_3$ nanoparticles calcined at different temperatures.

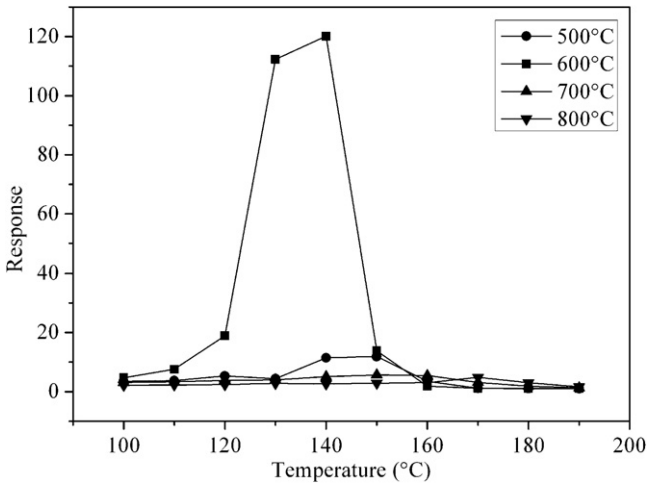

Fig. 4. Responses of $LaCo_{0.1}Fe_{0.9}O_3$ nanoparticles calcined at different temperatures to 500 ppm ethanol.

mic peak at 432.7 °C can be ascribed to the decomposition of the nitrates [30]. Each peak corresponds to an appreciable mass loss in the temperature range of 120–480 °C in the TGA curve. The weak exothermic peak at 602 °C may be due to the crystallization because no obvious mass loss is shown in the TGA curve, which is consistent with the following XRD data.

The XRD patterns of $LaCo_{0.1}Fe_{0.9}O_3$ nanoparticles calcined at different temperatures are shown in Fig. 3. After being calcined at 400 °C, the sample still remains amorphous. When the calcination temperature is increased to 600 °C, the amorphous metal oxide completely transformed to stable perovskite nanocrystallite, which is in good agreement with the DTA–TGA data above. For the samples calcined at 600, 700, and 800 °C, all the diffraction peaks correspond to the orthorhombic $LaFeO_3$ structure (JCPDC card no. 37-1493) [31]. It can be also observed that with an increase in the calcination temperature, the intensity of the peak increase significantly along with the reduction in the peak half width, indicating the growth of $LaCo_{0.1}Fe_{0.9}O_3$ nanoparticles with the calcination temperature. The crystallite sizes determined by the Scherrer equation are about 13, 15.1, 22, and 30 nm for the samples calcined at 500, 600, 700, and 800 °C, respectively [32].

The dependence of the response of the $LaCo_{0.1}Fe_{0.9}O_3$ nanoparticles calcined at different temperatures to 500 ppm ethanol on the operating temperature is shown in Fig. 4. The samples calcined at 500 and 600 °C exhibit the maximum response values at 140 °C. At this operating temperature, the response increases from 11.4 to 120.1 as the calcination temperature is raised from 500 to 600 °C, and then decreases with further increase in the calcination temperature. The samples calcined at 700 and 800 °C are almost not response to ethanol at all the tests. The calcination in air renders more oxygen vacancy generation, which enhances the gas response [33–35]. However, when the calcination temperature is higher than 600 °C, the crystallite size of $LaCo_{0.1}Fe_{0.9}O_3$ nanoparticles becomes larger due to agglomeration and therefore the specific surface area decreases, which will lead to the decrease of the gas response [22]. Accordingly, 600 °C is found to be the optimal calcination temperature for $LaCo_{0.1}Fe_{0.9}O_3$ nanoparticles, and all the samples used in the following experiments are calcined at this temperature.

3.2. Effect of Co-doping

The XRD patterns of $LaCo_xFe_{1-x}O_3$ (x = 0, 0.1, 0.2, and 0.3) nanoparticles calcined at 600 °C for 2 h is shown in Fig. 5. All the diffraction peaks correspond to the orthorhombic $LaFeO_3$ structure (JCPDC card no. 37-1493) [31], suggesting doping Co does not change the crystalline structure at these low doping rates. The Co concentration in $LaCo_xFe_{1-x}O_3$ has remarkable effects on the crystallite size. The crystallite sizes determined by the Scherrer equation are about 16.2, 15.1, 14.2, and 13.4 nm for $LaFeO_3$, $LaCo_{0.1}Fe_{0.9}O_3$, $LaCo_{0.2}Fe_{0.8}O_3$, and $LaCo_{0.3}Fe_{0.7}O_3$ nanoparticles, respectively [32]. The results suggest that the Co doping acts as a crystallite growth inhibitor for the $LaCo_xFe_{1-x}O_3$ material [36]. This is because the valence of dopant Co^{2+} is lower than that of Fe^{3+}. When the trivalent Fe^{3+} ions in $LaFeO_3$ are replaced by divalent Co^{2+} to form $LaCo_xFe_{1-x}O_3$, the charge neutrality is maintained by the formation of oxygen vacancies or the valence change of transition metal ions (like Fe^{4+}/Fe^{3+} or Co^{3+}/Co^{2+}), and these effects will restrain the growth of grains eventually [16,36–39]. In addition, the position of the orthorhombic structure peaks can be found to shift to higher angles with increasing the Co doping rate. This shift can be explained by the transformation from the orthorhombic perovskite structure of $LaFeO_3$ to the rhombohedral perovskite structure of $LaCoO_3$ (JCPDS 48-0123), resulting from the alignment distortion of the octahedral coordination by the gradual substitution of Fe by Co [17,36–39].

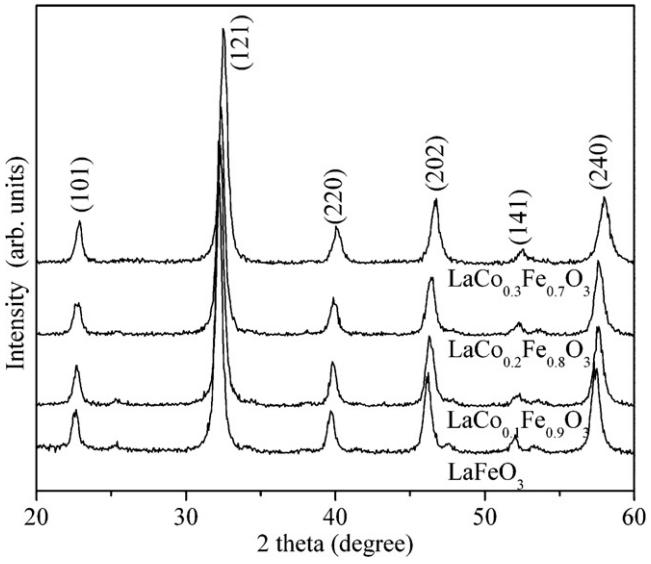

Fig. 5. XRD patterns of $LaFeO_3$, $LaCo_{0.1}Fe_{0.9}O_3$, $LaCo_{0.2}Fe_{0.8}O_3$, and $LaCo_{0.3}Fe_{0.7}O_3$ nanoparticles.

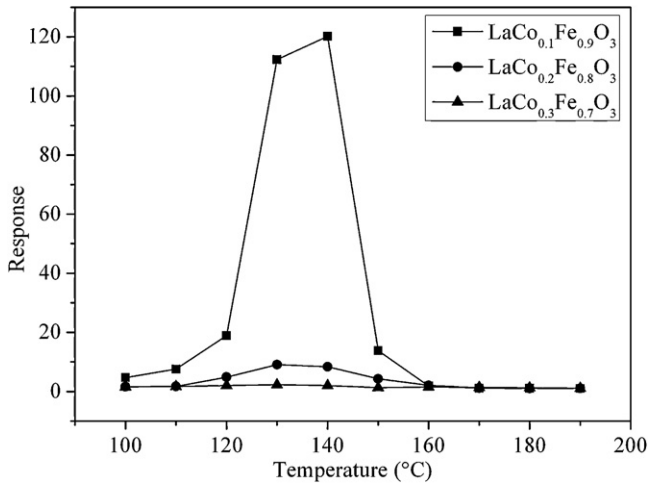

Fig. 6. Responses of $LaFeO_3$, $LaCo_{0.1}Fe_{0.9}O_3$, $LaCo_{0.2}Fe_{0.8}O_3$, and $LaCo_{0.3}Fe_{0.7}O_3$ nanoparticles to 500 ppm ethanol at different temperatures.

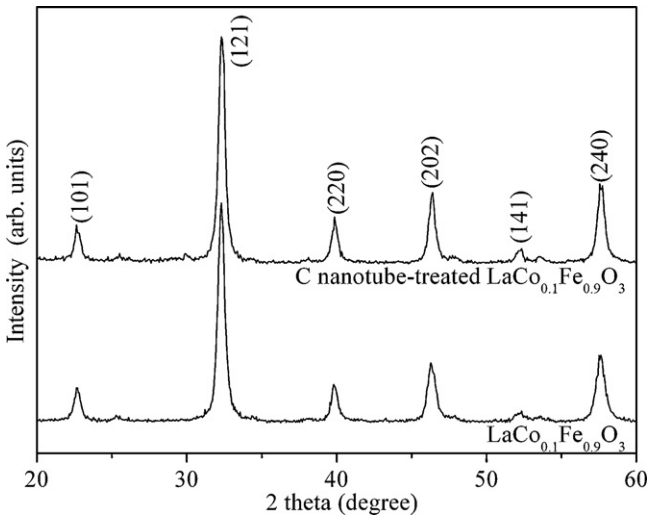

Fig. 7. XRD patterns of untreated and C nanotube-treated $LaCo_{0.1}Fe_{0.9}O_3$ nanoparticles.

The resistances of $LaFeO_3$, $LaCo_{0.1}Fe_{0.9}O_3$, $LaCo_{0.2}Fe_{0.8}O_3$, and $LaCo_{0.3}Fe_{0.7}O_3$ nanoparticles at 140 °C in air is about 60.2 MΩ, 144 kΩ, 5.4 kΩ, and 4.7 kΩ, respectively. The results reveal that doping Co can effectively reduce the resistance of $LaCo_xFe_{1-x}O_3$ nanoparticles. Using Kroger–Vink defect notations [40–42], when Fe^{3+} is replaced by Co^{2+}, the hole will be produced by the ionization of Co_{Fe}^{x}:

$$Co_{Fe}^{x} \rightarrow Co_{Fe}^{\prime} + h^{\bullet} \quad (1)$$

In this formula, Co_{Fe}^{x} means the point defect, which is produced when Co^{2+} occupies the sites of Fe^{3+} in the crystal. It indicates that doping Co^{2+} can increase the hole concentration in $LaFeO_3$. Since $LaCo_xFe_{1-x}O_3$ nanoparticles are p-type semiconducting materials, an increase of hole concentration results in a decrease of resistance.

The response of $LaFeO_3$ nanoparticles to 500 ppm ethanol can not be measured by our analysis system due to its very large resistance (over 500 MΩ) in ethanol ambience. The responses of other samples shown in Fig. 6 indicate that the near-optimal doping rate is 0.1. The corresponding sample ($LaCo_{0.1}Fe_{0.9}O_3$) exhibits the highest response value of about 120.1, which is 13.2 times larger than that of $LaCo_{0.2}Fe_{0.8}O_3$ (9.1) and 52.2 times larger than that of $LaCo_{0.3}Fe_{0.7}O_3$ (2.3). The highest response value of $LaCo_{0.1}Fe_{0.9}O_3$ nanoparticles can be explained by the suitable Co doping rate and appropriate resistance, which are discussed in the gas sensing mechanism part.

3.3. Effect of CNT-treatment

The XRD patterns of untreated $LaCo_{0.1}Fe_{0.9}O_3$ nanoparticles and CNT-treated $LaCo_{0.1}Fe_{0.9}O_3$ nanoparticles are shown Fig. 7. No diffraction peaks from any other impurities are detected, indicating all the CNTs have been removed during the calcination in 600 °C for 2 h. By employing the CNT-treatment, the crystallite sizes of the $LaCo_{0.1}Fe_{0.9}O_3$ are increased from 15.1 to 16.2 nm (determined by the Scherrer equation) [32], which is consistent with the SEM results shown below.

Fig. 8(a) and (b) shows the SEM micrographs of un-treated $LaCo_{0.1}Fe_{0.9}O_3$ nanoparticles and CNT-treated $LaCo_{0.1}Fe_{0.9}O_3$ nanoparticles, respectively. Compared with un-treated sample, CNT-treated $LaCo_{0.1}Fe_{0.9}O_3$ nanoparticles exhibit much larger crystallite size. The results indicate that CNT can promote the crystallite growth of $LaCo_{0.1}Fe_{0.9}O_3$, which can be explained by the exothermic oxidation reaction of CNTs. Moreover, for un-treated $LaCo_{0.1}Fe_{0.9}O_3$ nanoparticles, aggregation growth among the nanoparticles is clearly observed, and this aggregation structure will lead to a degradation of sensing response [43]. On the other hand, CNT-treated $LaCo_{0.1}Fe_{0.9}O_3$ nanoparticles exhibit obvious nanoporous structure, which thereby can be considered as the ideal morphology to show good sensing properties [44].

The average pore diameter, and BET surface area of the un-treated and CNT-treated $LaCo_{0.1}Fe_{0.9}O_3$ nanoparticles are listed in Table 1. After CNT-treatment, the average pore diameter increases, but the BET surface area decreases instead. These results are in good

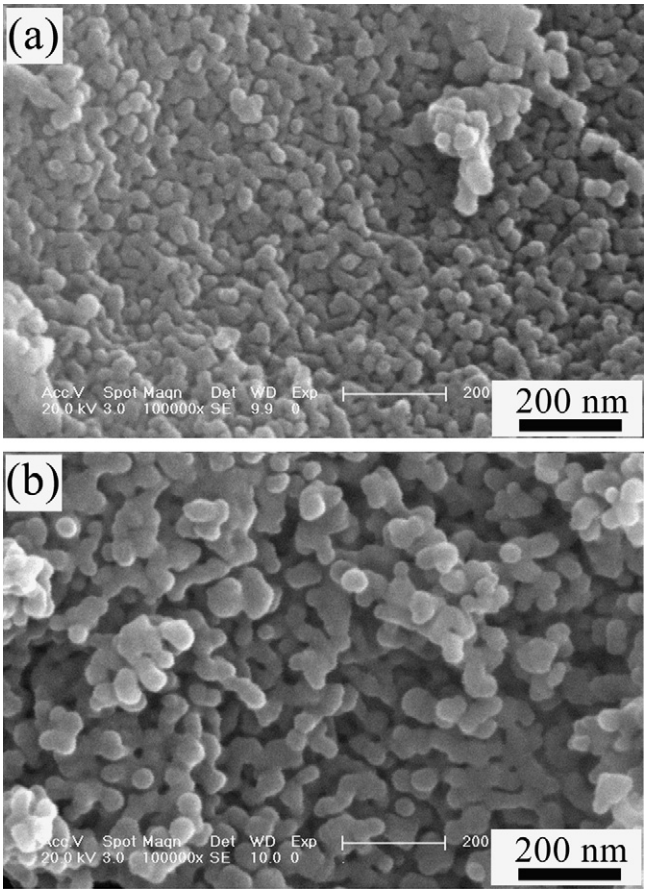

Fig. 8. SEM images of un-treated $LaCo_{0.1}Fe_{0.9}O_3$ nanoparticles (a) and C nanotube-treated $LaCo_{0.1}Fe_{0.9}O_3$ nanoparticles (b).

Table 1
Average pore diameter and BET surface area of the $LaCo_{0.1}Fe_{0.9}O_3$ nanoparticles with and without C nanotube-treatment.

Sample	Average pore diameter (Å)	BET (m^2/g)
Un-treated $LaCo_{0.1}Fe_{0.9}O_3$	163.0	53.1
C nanotube-treated $LaCo_{0.1}Fe_{0.9}O_3$	204.9	35.5

agreement with the SEM characterization. The CNT-treatment will increase the crystallite growth, leading to a large particle size and resulting in a lower BET surface area. The increased pore diameter is related to the removed CNT in the $LaCo_{0.1}Fe_{0.9}O_3$ precursor.

The response and recovery curves of un-treated and CNT-treated $LaCo_{0.1}Fe_{0.9}O_3$ nanoparticles are shown in Fig. 9. CNT treatment can effectively accelerate the reaction of $LaCo_{0.1}Fe_{0.9}O_3$ and gas molecules. The response and recovery times of un-treated $LaCo_{0.1}Fe_{0.9}O_3$ nanoparticles are about 56 and 95 s, respectively. While treated $LaCo_{0.1}Fe_{0.9}O_3$ nanoparticles exhibit much shorter response time (10 s) and recovery time (35 s). Moreover, CNT-treatment can also increase the response of $LaCo_{0.1}Fe_{0.9}O_3$. The response values of un-treated and treated $LaCo_{0.1}Fe_{0.9}O_3$ are about 120.1 and 137.3, respectively.

It is widely accepted that smaller sizes will lead to larger surface-to-volume rates, which will make the sensing materials absorb more target gases, and exhibit higher responses. However, the experimental results based on un-treated and CNT-treated $LaCo_{0.1}Fe_{0.9}O_3$ nanoparticles are not consisted with this rule. Besides the nanoporous structure mentioned above, the aggregation growth is more imaginable to happen among the un-treated $LaCo_{0.1}Fe_{0.9}O_3$ nanoparticles with smaller particle size. And this aggregation growth will restrict the sensing properties markedly [22].

Fig. 10 shows the response versus ethanol concentration of CNT-treated $LaCo_{0.1}Fe_{0.9}O_3$ nanoparticles at 140 °C. It can be seen that the response increases with increasing the ethanol concentration: in the low concentration range (from 50 to 400 ppm), the increase in the response depends near linearly on the concentration, while the response increases slowly in the range of 400–1000 ppm, and is gradually saturated at above 1000 ppm. The response values are about 10.1, 23.2, 56.5, 84.7, 120, 137.3, 150, 159, 165, 171, and 176 to 50, 100, 200, 300, 400, 500, 600, 700, 800, 900, and 1000 ppm ethanol, respectively.

In fact, the response of the semiconducting oxide gas sensor can usually be empirically represented as $R = A[C]^N + B$, where A and B are constants and [C] is the concentration of the target gas. N

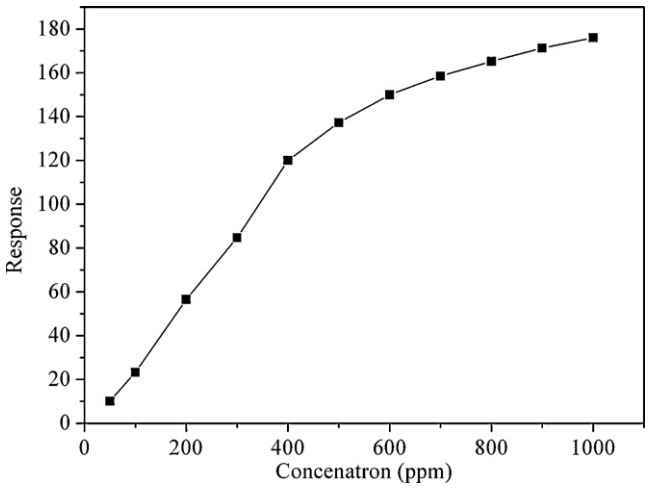

Fig. 10. Response of C nanotube-treated $LaCo_{0.1}Fe_{0.9}O_3$ nanoparticles vs ethanol concentration at 140 °C.

depends on the charge of the surface species and the stoichiometry of the elementary reactions on the surface [45]. For the CNT-treated $LaCo_{0.1}Fe_{0.9}O_3$ nanoparticles, N is calculated to be 1.24, meaning the change of response is strongly affected by the increase in ethanol concentration [2].

The CNT-treated $LaCo_{0.1}Fe_{0.9}O_3$ nanoparticles show different response values to different gases as the temperature varied (Fig. 11), which can be explained from the kinetics and mechanics of gas adsorption and desorption on the surface of $LaCo_{0.1}Fe_{0.9}O_3$ or similar semiconducting oxides [28]. At 140 °C, CNT-treated $LaCo_{0.1}Fe_{0.9}O_3$ nanoparticles show very low response to CH_3OH, CH_3COCH_3, and HCHO, and totally insensitive to petrol, C_6H_6, and C_2H_2, indicating its good selectivity.

3.4. Gas sensing mechanism

$LaCo_xFe_{1-x}O_3$ nanoparticles are p-type semiconducting materials in air. The resistances of these materials are related to oxygen [1]. In air ambient, $LaCo_xFe_{1-x}O_3$ nanoparticles will adsorb the oxygen molecule on the surface. The adsorbed oxygen is changed into various chemical absorptive states by trapping electrons from the bulk. Among those surface adsorptive states, there are following

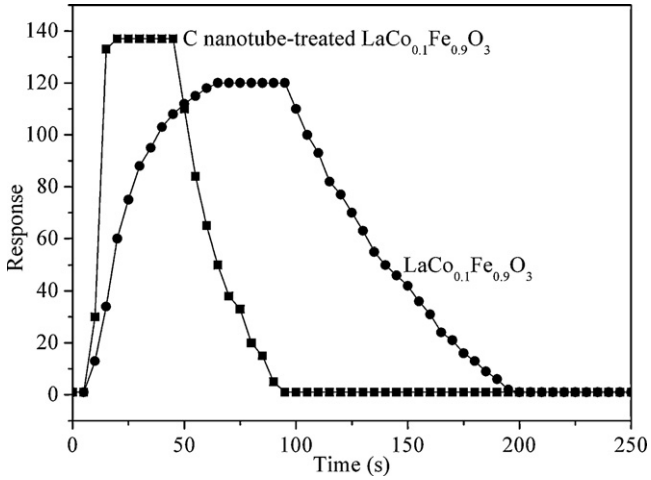

Fig. 9. Response and recovery curves of $LaCo_{0.1}Fe_{0.9}O_3$ nanoparticles (with and without C nanotube-treatment) to 500 ppm ethanol at 140 °C.

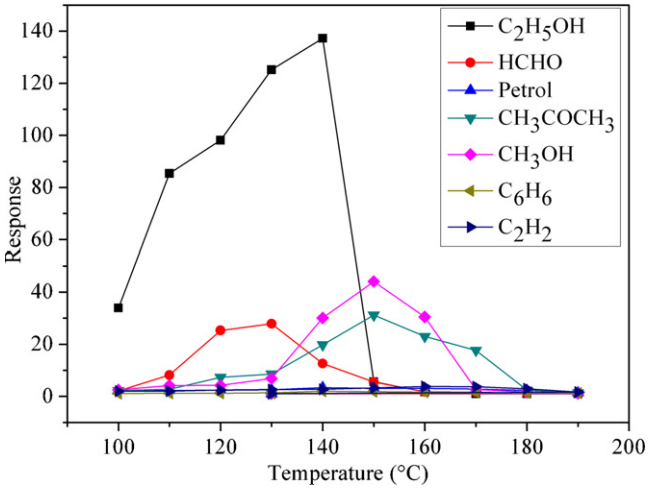

Fig. 11. Responses of C nanotube-treated $LaCo_{0.1}Fe_{0.9}O_3$ nanoparticles to 500 ppm different gases.

equilibria [46–48]:

$$O_2 + e^- \leftrightarrow O_2^- \quad \text{(ads.)} \tag{2}$$

$$O_2^- + e^- \leftrightarrow 2O^- \quad \text{(ads.)} \tag{3}$$

$$O^- + e^- \leftrightarrow O^{2-} \quad \text{(ads.)} \tag{4}$$

This will decrease the barrier height for a hole to transport and thus $LaCo_xFe_{1-x}O_3$ nanoparticles will show a low resistance. When the $LaCo_xFe_{1-x}O_3$ nanoparticles are exposed to a reducing gas (such as ethanol) at a moderate temperature, the gas molecule reacts with the chemisorbed oxygen (O^- is believed to be the main reactant [43]), and the electrons will release back to the valence band with an increase in resistance. The overall reaction of ethanol molecule with chemisorbed oxygen in this case may take place as below [46–48]:

$$C_2H_5OH + O^- \leftrightarrow CO_2 + H_2O + e^- \tag{5}$$

The content and activation of the chemisorbed oxygen are affected by the temperature, and the energy needed for the reaction between oxygen and gas molecules are also different, thus $LaCo_xFe_{1-x}O_3$ nanoparticles exhibit good selectivity at 140 °C (Fig. 11).

CNT is a 1D nanomaterial and can be totally removed in the calcination process [27]. Thus doping some CNT in precursors may create some 1D nanoporous structures with large pore diameter and high length to diameter rate. The sensing improvement by CNT-treatment is mainly observed in the response and recovery speeds, the much shorter response and recovery times brought by the CNT-treatment are attributed to the increased pore diameter, which is a base for gas molecule traveling through the sensing material [29]. The larger pore diameter will also enhance the response value, but this effect is limited by the lower BET surface area, which is caused by the increased particle size [22].

4. Conclusion

In summary, $LaCo_xFe_{1-x}O_3$ nanoparticles are prepared by a sol–gel method and their ethanol sensing properties are investigated. The optimal calcination temperature is found to be 600 °C, and the optimal doping rate (x) is found to be 0.1. It is also observed that adding CNTs in precursor of $LaCo_{0.1}Fe_{0.9}O_3$ nanoparticles can create some nanopores, thus enhance the response, and decrease the response and recovery times effectively. The results suggest that $LaCo_{0.1}Fe_{0.9}O_3$ nanoparticles are very promising materials for fabricating ethanol sensors. Meanwhile, the potential application of CNTs for pore-forming agent has also been demonstrated.

Acknowledgements

This research was financially supported by the National Natural Science Foundation of China (60977031), Jilin Provincial Science And Technology department (20060928, 20080330). Chinese National Programs for High Technology Research and Development (No. 2009AA03Z402), and Doctoral Found of Ministry of Education of China (20090061110040).

References

[1] J.W. Fergus, Perovskite oxides for semiconductor-based gas sensors, Sens. Actuators B: Chem. 123 (2007) 1169–1179.
[2] X. Liu, J. Hu, B. Cheng, H. Qin, M. Jiang, Acetone gas sensing properties of $SmFe_{1-x}Mg_xO_3$ perovskite oxides, Sens. Actuators B: Chem. 134 (2007) 483–487.
[3] E.L. Brosha, R. Mukundan, D.R. Brown, F.H. Garzon, J.H. Visser, M. Zanini, Z. Zhou, E.M. Logothetis, Co/HC sensors based on thin films of $LaCoO_3$ and $La_{0.8}Sr_{0.2}CoO_{3-\delta}$ metal oxides, Sens. Actuators B: Chem. 69 (2000) 171–182.
[4] A.V. Salker, N.-J. Choi, J.-H. Kwak, B.-S. Joo, D.D. Lee, Thick films of In, Bi and Pd metal oxides impregnated in $LaCoO_3$ perovskite as carbon monoxide sensor, Sens. Actuators B: Chem. 106 (2005) 461–467.
[5] L. Armelao, D. Barreca, G. Bottaro, A. Gasparotto, C. Maragno, E. Tondello, Hybrid chemical vapor deposition/sol–gel route in the preparation of nanophasic $LaCoO_3$ films, Chem. Mater. 17 (2005) 427–433.
[6] V.V. Kharton, A.A. Yaremchenko, E.N. Naumovich, Research on the electrochemistry of oxygen ion conductors in the former Soviet Union. II. Perovskite-related oxides, J. Solid State Electrochem. 3 (1999) 303–326.
[7] L.B. Kong, Y.S. Shen, Gas-sensing property and mechanism of $Ca_xLa_{1-x}FeO_3$ ceramics, Sens. Actuators B: Chem. 30 (1996) 217–221.
[8] A.D. Paoli, A.A. Barresi, Deep oxidation kinetics of trieline over $LaFeO_3$ perovskite catalyst, Ind. Eng. Chem. Res. 40 (2001) 1460–1464.
[9] U. Russo, L. Nodari, M. Faticanti, V. Kuncser, G. Filoti, Local interactions and electronic phenomena in substituted $LaFeO_3$ perovskites, Solid State Ionics 176 (2005) 97–102.
[10] P. Song, H. Qin, L. Zhang, K. An, Z. Lin, J. Hu, M. Jiang, The structure, electrical and ethanol-sensing properties of $La_{1-x}Pb_xFeO_3$ perovskite ceramics with $x \leq 0.3$, Sens. Actuators B: Chem. 104 (2005) 312–316.
[11] X. Liu, B. Cheng, J. Hu, H. Qin, M. Jiang, Semiconducting gas sensor for ethanol based on $LaMg_xFe_{1-x}O_3$ nanocrystals, Sens. Actuators B: Chem. 109 (2008) 53–58.
[12] H. Suo, F. Wu, Q. Wang, G. Liu, F. Qiu, B. Xu, M. Zhao, Study on ethanol sensitivity of nanocrystalline $La_{0.7}Sr_{0.3}FeO_3$-based gas sensor, Sens. Actuators B: Chem. 45 (1997) 245–249.
[13] F.J. Berry, X. Ren, J.R. Gancedo, J. Marco, Fe mössbauer spectroscopy study of $LaFe_{1-x}Co_xO_3$ (x = 0 and 0.5) formed by mechanical milling, Hyperfine Interact. 156/157 (2004) 335–340.
[14] V. Szabo, M. Bassir, A.V. Neste, S. Kaliaguine, Perovskite-type oxides synthesized by reactive grinding. Part IV. Catalytic properties of $LaCo_{1-x}Fe_xO_3$ in methane oxidation, Appl. Catal. B: Environ. 43 (2003) 81–92.
[15] X. Ge, Y. Liu, X. Liu, Prepartion and gas sensitive properties of $LaFe_{1-y}Co_yO_3$ semiconducting materials, Sens. Actuators B: Chem. 79 (2001) 171–174.
[16] Z. Wang, C. Chen, C. Feng, J. Wang, B. Zou, M. Zhao, F. Wu, Synthesis, Characterization and humidity sensitive properties of nanocrystalline $LaCo_xFe_{1-x}O_3$, Acta Phys. Chim. Sinica 24 (2008) 375–378.
[17] H. Cui, M. Zayat, D. Levy, Epoxide assisted sol–gel synthesis of perovskite-type $LaM_xFe_{1-x}O_3$ (M = Ni,Co) nanoparticles, J. Non-Cryst. Solids 325 (2006) 3035–3040.
[18] X.J. Huang, Y.K. Choi, Chemical sensors based on nanostructured materials, Sens. Actuators B: Chem. 122 (2007) 659–671.
[19] W. Li, N.D. Hoa, Y. Cho, D. Kim, J.S. Kim, Nanofibers of conducting polyaniline for aromatic organic compound sensor, Sens. Actuators B: Chem. 143 (2009) 132–138.
[20] O. Lupan, L. Chow, G. Chai, A single ZnO tetrapod-based sensor, Sens. Actuators B: Chem. 141 (2009) 511–517.
[21] A. Kolmakov, M. Moskovits, Chemical sensing and catalysis by one-dimensional metal-oxide nanostructures, Ann. Rev. Mater. Res. 34 (2004) 151–180.
[22] M.E. Franke, T.J. Koplin, U. Simon, Metal and metal oxide nanoparticles in chemiresistors: does the nanoscale matter? Small 2 (2006) 36–50.
[23] A.S. Adekunle, B.O. Agboola, J. Pillay, K.I. Ozoemena, Electrocatalytic detection of dopamine at single-walled carbon nanotubes–iron (III) oxide nanoparticles platform, Sens. Actuators B: Chem. 148 (2010) 93–102.
[24] H. Kang, S. Lim, N. Park, K.Y. Chun, S. Baik, Improving the sensitivity of carbon nanotube sensors by benzene functionalization, Sens. Actuators B: Chem. 147 (2010) 316–321.
[25] D.R. Kauffman, A. Star, Carbon nanotube gas and vapor sensors, Angew. Chem. Int. Ed. 47 (2008) 6550–6570.
[26] Y.X. Liang, Y.J. Chen, T.H. Wang, Low-resistance gas sensors fabricated from multiwalled carbon nanotubes coated with a thin tin oxide layer, Appl. Phys. Lett. 85 (2004) 666–668.
[27] N.V. Hieu, N.A.P. Due, T. Trung, M.A. Tuan, N.D. Chien, Gas-sensing properties of tin oxide doped with metal oxides and carbon nanotubes: a competitive sensor for ethanol and liquid petroleum gas, Sens. Actuators B: Chem. 144 (2010) 450–456.
[28] Q. Qi, T. Zhang, L. Liu, X. Zheng, Q. Yu, Y. Zeng, H. Yang, Selective acetone sensor based on dumbbell-like ZnO with rapid response and recovery, Sens. Actuators B: Chem. 134 (2008) 166–170.
[29] H. Zhang, Z. Li, L. Liu, X. Xu, Z. Wang, W. Wang, W. Zheng, B. Dong, C. Wang, Enhancement of hydrogen monitoring properties based on Pd–SnO_2 composite nanofibers, Sens. Actuators B: Chem. 147 (2010) 111–115.
[30] Z. Wang, C. Chen, T. Zhang, H. Guo, B. Zou, R. Wang, F. Wu, Humidity sensitive properties of K^+-doped nanocrystalline $LaCo_{0.3}Fe_{0.7}O_3$, Sens. Actuators B: Chem. 126 (2007) 678–683.
[31] Z. Yang, Y. Huang, B. Dong, H.L. Li, Controlled synthesis of highly ordered $LaFeO_3$ nanowires using a citrate-based sol–gel route, Mater. Res. Bull. 41 (2006) 274–281.
[32] Q. Qi, Y. Feng, T. Zhang, X. Zheng, G. Lu, Influence of crystallographic structure on the humidity sensing properties of KCl-doped TiO_2 nanofibers, Sens. Actuators B: Chem. 139 (2009) 611–617.
[33] M. Epifani, L. Francioso, P. Siciliano, A. Helwig, G. Mueller, R. Díaz, J. Arbiol, J.R. Morante, SnO_2 thin films from metalorganic precursors: synthesis characterization, microelectronic processing, Sens. Actuators B: Chem. 124 (2007) 217–226.
[34] F. Qiu, Q. Zhu, X. Yang, Y. Quan, B. Xu, Preparation of planar CO_2 sensor based on solid-electrolyte NASICON synthesized by sol–gel process, Mater. Chem. Phys. 83 (2004) 193–198.

[35] V. Jayaraman, E. Prabhu, K.I. Gnanasekar, T. Gnanasekaran, G. Perisawami, Soft-chemical preparation and gas sensing properties of iron and manganese substituted $Cr_{1.8}Ti_{0.2}O_{3+\delta}$, Mater. Chem. Phys. 86 (2004) 165–175.
[36] X. Liu, B. Cheng, J. Hu, H. Qin, M. Jiang, Semiconducting gas sensor for ethanol based on $LaMg_xFe_{1-x}O_3$ nanocrystals, Sens. Actuators B: Chem. 129 (2008) 53–58.
[37] Q. Ming, M.D. Nersesyan, A. Wagner, J. Ritchie, J.T. Richardson, D. Luss, A.J. Jacobson, Y.L. Yang, Combustion synthesis and characterization of Sr and Ga doped $LaFeO_3$, Solid State Ionics 122 (1999) 113–121.
[38] X. Qi, J. Zhou, Z. Yue, Z. Gui, L. Li, A simple way to prepare nanosized $LaFeO_3$ powders at room temperature, Ceram. Int. 29 (2003) 347–349.
[39] S. Zhao, J.K.O. Sin, B. Xu, M. Zhao, Z. Peng, H. Cai, A high performance ethanol sensor based on field-effect transistor using a $LaFeO_3$ nano-crystalline thin-film as a gate electrodem, Sens. Actuators B: Chem. 64 (2000) 83–87.
[40] L. Zhang, J. Hu, P. Song, H. Qin, M. Jiang, Electric properties and acetone-sensing characteristics of $La_{1-x}Pb_xFeO_3$ perovskite system, Sens. Actuators B: Chem. 114 (2006) 836–840.
[41] P. Porta, S. Cimino, S. De Rossi, M. Faticanti, G. Minelli, I. Pettiti, AFO_3 (A = La, Nd, Sm) $LaFe_{1-x}Mg_xO_3$ perovskites: structural and redox properties, Mater. Chem. Phys. 71 (2001) 165–173.
[42] P. Ciambelli, S. Cimino, S. De Rossi, L. Lisi, G. Minelli, P. Porta, G. Russo, $AFeO_3$ (A = La, Nd, Sm) and $LaFe_{1-x}Mg_xO_3$ perovskites as methane combustion and CO oxidation catalysts: structural, redox and catalytic properties, Appl. Catal. B 29 (2001) 239–250.
[43] Q. Qi, T. Zhang, L. Liu, X. Zheng, G. Lu, Improved NH3, C_2H_5OH, and CH_3COCH_3 sensing properties of SnO_2 nanofibers by adding block copolymer P123, Sens. Actuators B: Chem. 141 (2009) 174–178.
[44] Y. Wang, X. Jiang, Y. Xia, A solution-phase, precursor route to polycrystalline SnO_2 nanowires that can be used for gas sensing under ambient conditions, J. Am. Chem. Soc. 125 (2003) 16176–16177.
[45] Y.J. Chen, L. Nie, X.Y. Xue, Y.G. Wang, T.H. Wang, Linear ethanol sensing of SnO_2 nanorods with extremely high sensitivity, Appl. Phys. Lett. 88 (2005) 0831051/1–0831051/3.
[46] Y.L. Liu, Y. Xing, H.F. Yang, Z.M. Liu, Y. Yang, G.L. Shen, R.Q. Yu, Ethanol gas sensing properties of nano-crystalline cadmium stannate thick films doped with Pt, Anal. Chim. Acta 527 (2004) 21–26.
[47] X. Liu, B. Cheng, H. Qin, P. Song, S. Huang, R. Zhang, J. Hu, M. Jiang, Preparation, electrical and gas-sensing properties of perovskite-type $La_{1-x}Mg_xFeO_3$ semiconductor materials, J. Phys. Chem. Solids 68 (2007) 511–515.
[48] N. Barsan, D. Koziej, U. Weimar, Metal oxide-based gas sensor research: how to? Sens. Actuators B: Chem. 121 (2007) 18–35.

Biographies

Caihui Feng received the master degree in chemistry at Changchun Normal University in 2006. She has been studying at Jilin University since 2007, and is mainly devoted to the research of functional nanomaterials and chemical sensors.

Shengping Ruan received the PhD degree of electronic science and engineering from Jilin University in 2001. Now, he is mainly devoted to the research of electronic functional materials and devices.

Jiajing Li received the bachelor degree in chemistry at Jilin Normal University in 2009. She has been studying at Jilin University since 2009. She is mainly devoted to the research of functional nanomaterials and chemical sensors.

Bo Zou received the bachelor degree in chemistry at Jilin University in 2002. He has been studying at the same university since 2003. He is mainly devoted to the research of functional nanomaterials.

Junyu Luo received the bachelor degree in Jilin University in 2008. He has been studying at the same University since 2009, and is mainly devoted to the research of electronic functional materials and devices.

Weiyou Chen received the PhD degree of electronic science and engineering from Jilin University in 1992. Now, he is mainly devoted to the research of electronic functional materials and devices.

Wei Dong received the PhD degree of microelectronics and solid-state electronics from Jilin University in 2004. Now, she is mainly devoted to the research of electronic functional materials and devices.

Fengqing Wu graduated from the Jilin University in 1976. She has been working at Jilin University since 1977, and is mainly devoted to the research of functional nanomaterials.